Two-photon ionization of the neutral argon atom*

Michael S. Pindzola and Hugh P. Kelly
Department of Physics, University of Virginia, Charlottesville, Virginia 22901
(Received 20 January 1975)

The two-photon ionization cross section for the neutral argon atom is calculated. A double perturbation expansion in the Coulomb correlations and the atom–radiation-field interaction is made. Contributions from intermediate states are obtained by direct summation over Hartree-Fock bound and continuum single-particle states. The effects of electron correlations and photon-radiative corrections are investigated. Comparison is made with previous theoretical methods.

I. INTRODUCTION

The principles of multiphoton processes in atomic systems have been known since the early days of quantum mechanics.[1] With the advent of the laser, the experimental observation[2-5] of multiphoton processes has become possible. Renewed theoretical interest[6] has centered around the standard perturbation expansion in the photon-field–atom interaction Hamiltonian[7-11] and the very intense-radiation-field methods.[12-14]

The validity of perturbation theory itself extends to quite strong photon fields. One of the first accurate calculations of a two-photon ionization process was made by Zernik[7] on the metastable $2s$ hydrogen atom. The sums over intermediate states found in perturbation theory were explicitly evaluated by Zernik using the method of Schwartz and Tieman.[15] Bebb and Gold[8] applied approximate methods to calculate for hydrogen and the rare-gas atoms various ionization rates involving 2–12 photons. Double photodetachment of various negative halide ions has also been investigated.[16] The low ionization energy of the alkali metals has made possible experimental observation[4,5] of two- and three-photon processes using present-day chemical and glass lasers. Theoretical calculation[17] of multiphoton ionization rates of the alkalis is made easier as a result of the concentration of the oscillator strength in the low-lying bound excited states. Sums over intermediate states can thus be truncated to include only a few important bound states without much loss of accuracy.

At very intense photon fields the standard perturbation theory breaks down.[12] The semiclassical tunnel ionization method developed by Keldysh[18] and the momentum-translation method of Reiss[13] attempt to deal with the range of intensities at which the atomic and photon fields are nearly equal. At ultrastrong photon fields the electron-atom interaction can be treated as a perturbation on the laser-electron Hamiltonian.[14]

There are many interesting problems and features in the current theoretical work on multiphoton ionization using standard perturbation theory. Sums over intermediate states present a problem for those atomic systems in which the continuum plays a vital role. The Schwartz-Tieman method can be used with hydrogenic wave functions,[10] and a theory involving the Green's function of a complex atom has been developed.[19] Also being discussed is the question of how the ratio of the ionization rates of circular polarized light to linear polarized light behaves for higher-order multiphoton processes.[20,21] Higher-order photon radiative corrections to a particular two- or three-photon ionization process near resonance are also being investigated.[22,23]

In this paper we present a calculation for the two-photon ionization of the argon atom. Contributions from the intermediate states are obtained by direct summation over the Hartree-Fock bound and continuum single-particle states. The effects of electron correlations and higher-order photon radiative corrections are investigated. Although experiments involving two-photon ionization of argon await the development of x-ray lasers, the methods used in this paper can be generalized to yield accurate multiphoton ionization rates for any atom. In Sec. II we present the perturbation theory of the two-photon ionization of an atom; Sec. III contains the results of the argon calculation and a comparison with other theoretical methods; and Sec. IV contains a brief summary.

II. THEORY

The theory of the interaction of the electromagnetic field with matter is well known.[24] The Hamiltonian for an atomic system interacting with a radiation field may be written

$$H = H_{\text{atom}} + H_{\text{rad}} + H_{\text{int}} . \tag{1}$$

The Hamiltonian for an N-electron atom, H_{atom}, in configuration space may be given by

$$H_{\text{atom}} = H_{0A} + H_{\text{corr}} , \tag{2}$$

where

$$H_{0A} = \sum_{i=1}^{N} \left(-\tfrac{1}{2} \nabla_i^2 - Z/r_i + V_i \right) \tag{3}$$

and

$$H_{\text{corr}} = \sum_{i<j=1}^{N} v_{ij} - \sum_{i=1}^{N} V_i \,. \tag{4}$$

Atomic units are used throughout this paper. In Eqs. (3) and (4), V_i is some suitable single-particle potential, v_{ij} is the Coulomb interaction between pairs of electrons, and Z is the atomic number. The solution of the time-independent Schrödinger equation using H_{0A} of Eq. (3) may be expressed as a linear combination of determinants formed from the single-particle solutions ϕ_n of

$$\left(-\tfrac{1}{2} \nabla^2 - Z/r + V \right) \phi_n = \epsilon_n \phi_n \,. \tag{5}$$

The Hamiltonian of the atom may also be written as a quantized field using creation and annihilation operators for the states ϕ_n. The electromagnetic field may be quantized[25] to yield

$$H_{\text{rad}} = \frac{1}{8\pi} \int (\vec{E}^2 + \vec{H}^2)\, d\vec{r} \,, \tag{6}$$

where $\vec{E}$ and $\vec{H}$ are the electric and magnetic fields, respectively. The vector potential is given by

$$\vec{A}(\vec{r}) = \sum_{\lambda} \left(\hat{\epsilon}_\lambda a_\lambda e^{i \vec{k}_\lambda \cdot \vec{r}} + \hat{\epsilon}_\lambda^* a_\lambda^\dagger e^{-i \vec{k}_\lambda \cdot \vec{r}} \right), \tag{7}$$

where λ is the index of the photon mode. The solution of the Schrödinger equation using H_{rad} of Eq. (6) may be expressed in terms of photon occupation number states $|\, n_\lambda \rangle$ and the action of the annihilation and creation operators on them,

$$a_\lambda \,|\, n_\lambda \rangle = (2\pi c^2 n_\lambda / \omega_\lambda)^{1/2} \,|\, n_\lambda - 1 \rangle \,, \tag{8}$$

$$a_\lambda^\dagger \,|\, n_\lambda \rangle = [\, 2\pi c^2 (n_\lambda + 1)/\omega_\lambda]^{1/2} \,|\, n_\lambda + 1 \rangle \,, \tag{9}$$

where ω_λ is the angular frequency of the λth mode. The interaction Hamiltonian H_{int} is given by

$$H_{\text{int}} = \sum_{j=1}^{N} \left[-(i/c) \vec{A}(\vec{r}_j) \cdot \nabla_j + (1/2c^2) \,|\, \vec{A}(\vec{r}_j) \,|^2 \right]. \tag{10}$$

The second term of Eq. (10) involving $|\, \vec{A} \,|^2$ does not contribute in the dipole approximation. For notational simplicity we can consider a radiation field containing only one mode.

Transition rates in multiphoton ionization of atoms may be obtained from time-dependent perturbation theory using the Brueckner[26]-Goldstone[27] linked-cluster expansion. The unperturbed Hamiltonian is given by

$$H_0 = H_{0A} + H_{\text{rad}} \,, \tag{11}$$

and its eigenstates $|\, \Phi_j^n \rangle$ are products of an electronic state $|\, \Phi_j \rangle$ and a radiation state with n photons. The perturbation is then

$$H_1 = H_{\text{int}} + H_{\text{corr}} \,. \tag{12}$$

The solution $\Psi(t)$ of the time-dependent Schrödinger equation,

$$\frac{i \partial \Psi(t)}{\partial t} = H \Psi(t) \,, \tag{13}$$

may be expressed using the adiabatic hypothesis[28] as

$$\Psi(t) = \lim_{\alpha \to 0} \frac{e^{-iH_0 t} U_\alpha(t) \,|\, \Phi_0^n \rangle}{\langle\, \Phi_0^n \,|\, U_\alpha(t) \,|\, \Phi_0^n \rangle} \,. \tag{14}$$

The time-evolution operator[29] $U_\alpha(t)$ is explicitly written

$$U_\alpha(t) = 1 + \frac{1}{i} \int_{-\infty}^{t} H_1(\tau)\, d\tau + \frac{1}{i^2} \int_{-\infty}^{t} d\tau \int_{-\infty}^{\tau} d\tau' H_1(\tau) H_1(\tau') + \cdots \,, \tag{15}$$

where

$$H_1(t) \equiv e^{iH_0 t} H_1 e^{\alpha t} e^{-iH_0 t} \,. \tag{16}$$

The probability W that a transition has taken place from the ground state $|\, \Phi_0^n \rangle$ to the final state $|\, \Phi_f^m \rangle$ is given by

$$W = |\, M \,|^2 / \langle \Psi \,|\, \Psi \rangle \,, \tag{17}$$

where

$$M = \langle \Phi_f^m(t) \,|\, \Psi(t) \rangle \,. \tag{18}$$

The denominator of Eq. (17) is needed to normalize $|\, \Psi(t) \rangle$. Corrections to unity in $\langle \Psi \,|\, \Psi \rangle$ are second order in the Coulomb interaction, and thus they should have a fairly small effect on the transition probability (2.3% for photoabsorption by argon[30]). For the two-photon ionization of an atom, contributions to the matrix element M come from second- and higher-order terms in the expansion of $U_\alpha(t)$ in Eq. (15). Carrying out the time integrations, one has

$$M_2 = \lim_{\alpha \to 0} \langle \Phi_f^{n-2} \,|\, \sum_{m=2}^{\infty} \frac{\exp[-i(E_0^n - H_0 + mi\alpha)t]}{E_0^n - H_0 + mi\alpha} H_1 \cdots \frac{1}{E_0^n - H_0 + i\alpha} H_1 \,|\, \Phi_0^n \rangle \langle \Phi_0^n \,|\, U_\alpha(t) \,|\, \Phi_0^n \rangle^{-1} \,. \tag{19}$$

By the use of Wick's theorem,[31] the numerator of Eq. (19) becomes a sum of terms which may be represented by Goldstone diagrams. The denominator of Eq. (19) cancels the unlinked clusters. The transition rate w may then be expressed as[32]

$$w = 2\pi\delta(E_0^n - E_f^{n-2}) \left| \langle \Phi_f^{n-2} \mid \sum_L H_1 \cdots \frac{1}{E_0^n - H_0} H_1 \mid \Phi_0^n \rangle \right|^2 \langle \Psi \mid \Psi \rangle^{-1}, \tag{20}$$

where $\sum_L$ means that only linked diagrams are to be included.

Techniques developed in previous applications[33] of the Brueckner-Goldstone expansion may be used to evaluate Eq. (20). Representative diagrams from each order are shown in Fig. 1. The solid dots indicate an absorptive interaction with the radiation field, the open dots are emission processes, and the dashed lines not ending in dots represent Coulomb interactions. The order of the diagram is simply the total number of interactions, either Coulomb or radiation. Figures 1(a) and 1(b) are the only second-order terms leading to two-photon ionization. The third-order diagrams of Figs. 1(c)–1(e) show how the time orderings of the Coulomb interaction can vary. There are many more third-order diagrams that are not shown in Fig. 1 which contribute to the two-photon process. Figure 1(f) is a pure radiative fourth-order term. In a high-flux electromagnetic field the electron that is being ionized by the two-photon process may use as an intermediate process the emission and absorption of a photon of the radiation field (or the reverse). The open dot of Fig. 1(f) may have four possible time orderings, thus leading to different energy denominators. It should also be noted that due to the two extra interactions with the radiation field, Fig. 1(f) is of a higher flux dependence than the second- or third-order terms shown. For high photon-flux rates a perturbation-theory treatment of two-photon ionization will break down. Figure 1(g) is just one of the many fourth-order Coulomb correlation terms. Poles in the denominators of the diagrams of Fig. 1 are of two types. In the two-photon ionization of an atom, certain values of photon energy ω can permit single-photon absorption from a ground electronic state to a low-lying bound excited state. This process gives rise to radiation resonances. Another type of resonant process occurs when a bound electronic configuration is degenerate in energy with a two-photon continuum configuration. These are autoionization resonances. In both cases an appropriate half-width and level shift can be introduced in the denominator to remove the pole. Further discussion of resonances is reserved for Sec. III.

The single-particle excited states used in the diagrams of Fig. 1 are calculated by using Eq. (5) with various spherically symmetric Hartree-Fock V^{N-1} potentials for $V(r)$ such that

$$\langle \vec{r} \mid k \text{ or } n, l, m_l, m_s \rangle = R(k \text{ or } n, l; r) \times Y_{lm}(\theta, \phi)\chi_s(m_s), \tag{21}$$

where $Y_{lm}(\theta, \phi)$ is a spherical harmonic and $\chi_s(m_s)$ is the spin function. Each diagram is thus analyzed into its various angular momentum excitation components. Each excitation component itself involves an angular summation over m_l and m_s as well as radial integrations over the various Coulomb and radiation-field interactions. The continuum states are normalized according to

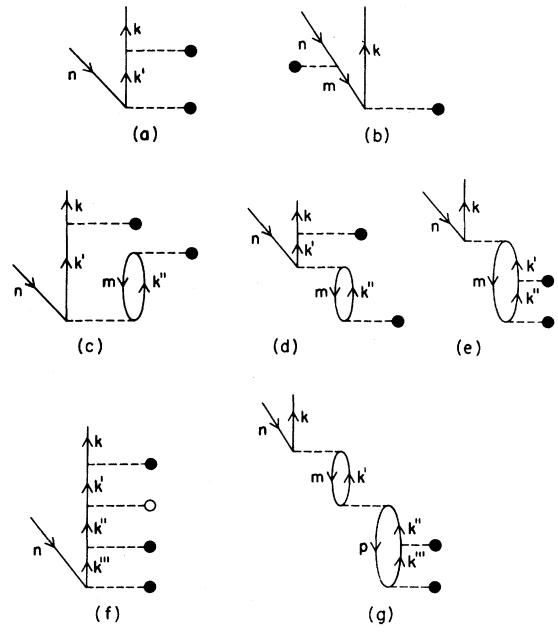

FIG. 1. Diagrams contributing to a two-photon process that occur in the perturbation expansion for the atom and radiation field. Solid dots indicate an absorptive interaction with the radiation field, circles indicate emission, while the dashed lines not ending in dots represent Coulomb interactions. The order of the diagram is simply the number of interactions. Figures (a) and (b) are the only second-order terms. Figures (c), (d), and (e) are examples of ground-state, intermediate-state, and final-state third-order correlation diagrams. Figure (f) is a pure radiative fourth-order diagram while Fig. (g) is a fourth-order correlation diagram.

$$R(k, l; r) \to \sin[kr + \delta_l + (q/k)\ln(2kr) - \tfrac{1}{2}l\pi]/r \quad \text{as } r \to \infty, \quad (22)$$

where $V(r) \to q/r$. As discussed by Amus'ya *et al.*[34] and others,[35] the appropriate V^{N-1} potential $V(r)$ is obtained by coupling the excited orbital to the LS-coupled core states to form various LS states. In the case of a single dipole interaction with a closed-shell ground state, the potential $V(r)$ is that for a ^1P many-particle excited state. For two dipole interactions, the resulting many-particle excited state is ^1D or ^1S, with the corresponding potential for each case. The single-particle potentials obtained in this manner cancel not only diagrams having interactions with the passive unexcited states but also important intrashell correlation diagrams.

Using the normalization of the continuum-state functions of Eq. (22), the density of states with respect to energy is

$$\rho_\epsilon = 2/\pi k , \quad (23)$$

where k is the outgoing electron's momentum. In the dipole approximation, the lowest-order cross section for two-photon ionization is obtained by using Eqs. (20) and (23) along with Figs. 1(a) and 1(b) to yield

$$\sigma = \frac{16\pi^2 F}{\omega^2 c^2 k}\left| \sum\!\!\!\!\!\!\int_{k'} \frac{\langle k|\hat{\epsilon}\cdot\nabla|k'\rangle\langle k'|\hat{\epsilon}\cdot\nabla|n\rangle}{\epsilon_n - \epsilon_{k'} + \omega} - \frac{\langle k|\hat{\epsilon}\cdot\nabla|m\rangle\langle m|\hat{\epsilon}\cdot\nabla|n\rangle}{\epsilon_m - \epsilon_k + \omega}\right|^2 , \quad (24)$$

where $F = nc$ is the photon flux, ϵ_k is the energy for the single-particle state $|k\rangle$, higher-order diagrams add to the terms inside the absolute square, and $\sum\!\!\!\!\!\!\int$ represents a sum over bound states and an integration over the continuum.

III. RESULTS

For the two-photon ionization of the $3p$ shell of argon, the second-order diagram in Fig. 1(a) may be written

$$D(kl) = \sum_{l'}\left(\sum_{n'} \frac{\langle kl|J|n'l'\rangle\langle n'l'|J|3p\rangle}{\epsilon_{3p} - \epsilon_{n'l'} + \omega} + \frac{2}{\pi}\int_0^\infty dk' \frac{\langle kl|J|k'l'\rangle\langle k'l'|J|3p\rangle}{\epsilon_{3p} - \tfrac{1}{2}k'^2 + \omega}\right), \quad (25)$$

where the factor $2/\pi$ arises from the normalization of Eq. (22). The sum over bound states n' is carried out explicitly for ten or so excited states (for each l' value) and the remaining infinite sum is estimated by the n^{-3} rule.[33] J represents the dipole operator in the length or velocity form. From angular momentum selection rules $l' = 0$ and 2 for $l = 1$, and $l' = 2$ for $l = 3$. The energy of the ionized electron in a single-particle picture is given by

$$\epsilon_{kl} = \tfrac{1}{2}k^2 = \epsilon_{3p} + 2\omega . \quad (26)$$

The complete set of radial functions $n's$ and $k's$ were obtained using the Hartree-Fock V^{N-1} potential for the $(3p)^5 ks\,^1P$ state. The $n'd$ and $k'd$ functions were obtained using the potential for the $(3p)^5 kd\,^1P$ state. The final continuum states at the energies given by Eq. (26) were calculated using the HF V^{N-1} potential for the $(3p)^5 kf\,^1D$, $(3p)^5 kp\,^1D$, and $(3p)^5 kp\,^1S$ many-particle states. The Silverstone-Huzinaga potential[36,37] was used to guarantee the orthogonality between excited and core states for the $ks\,^1P$ and $kp\,^1D$ states. Schmidt orthogonalization was used for the $kp\,^1S$ states.

The sum over bound and continuum excited states in Eq. (25) was made explicitly. The matrix elements $\langle kl|J|n'l'\rangle$ and $\langle kl|J|k'l'\rangle$ were evaluated by truncating the radial integration at a fixed value R. If the cross section is computed using Eq. (25) for various cutoff values R, it becomes convergent as R is increased. In this paper $R = 20.365$ bohr was used. It may be noted that the radial probability distribution function for the Hartree-Fock $3p$ state of argon has a peak value of 0.67 at 1.4 bohr and is less than 10^{-6} by 9.1 bohr. The cutoff at $R = 20.365$ is sufficient to accurately calculate $\langle kl|J|n'l'\rangle$ for several low-lying bound excited states. The number of mesh points in k' space needed to provide proper evaluation of the continuum integral in Eq. (25) was determined by a sum-rule check. The quantity (in the length formulation with linear polarization)

$$L(kl) = \sum_{l'}\left(\sum_{n'}\langle kl|z|n'l'\rangle\langle n'l'|z|3p\rangle + \frac{2}{\pi}\int_0^\infty dk'\langle kl|z|kl'\rangle\langle k'l'|z|3p\rangle\right) \quad (27)$$

was evaluated and compared to the collapsed integral $\langle kl|z^2|3p\rangle$. Results of this comparison at $R = 20.365$ with a 76-point k'-space mesh are given in Table I for the three final states $kf\,^1D$, $kp\,^1D$, and $kp\,^1S$ involved in the two-photon ionization of argon. It was found that increasing the radial cutoff point R beyond 20.365 bohr results in a substantial increase in the number of k'-space mesh points needed to properly evaluate the continuum integrals and therefore a considerable increase in computing cost.

Results for the two-photon ionization of argon in lowest order are shown in Figs. 2–4. Calcula-

TABLE I. Comparison between $L(kl)$ and $\langle kl|z^2|3p\rangle$ for $R = 20.365$ bohr.

A. $kf\ ^1D$ final state

ω (eV)	$\langle kf\|z^2\|3p\rangle_{\text{radial}}$ (a.u.) [a]	$L(kf)^{l'=2}_{\text{radial}}$ (a.u.) [a]
9	−3.609	−3.523
10	−4.613	−4.607
11	−5.145	−5.167
12	−5.390	−5.380
13	−5.458	−5.456
15.25	−5.261	−5.250

B. $kp\ ^1D$ final state

ω (eV)	$\langle kp\|z^2\|3p\rangle_{\text{radial}}$ (a.u.) [b]	$L(kp)^{l'=0}_{\text{radial}}$ (a.u.) [b]	$L(kp)^{l'=2}_{\text{radial}}$ (a.u.) [b]
9	−2.930	−2.892	−2.984
10	−2.839	−2.794	−2.863
11	−2.628	−2.710	−2.606
12	−2.402	−2.424	−2.402
13	−2.189	−2.127	−2.193
15.25	−1.786	−1.862	−1.796

C. $kp\ ^1S$ final state

ω (eV)	$\langle kp\|z^2\|3p\rangle_{\text{radial}}$ (a.u.) [b]	$L(kp)^{l'=0}_{\text{radial}}$ (a.u.) [b]	$L(kp)^{l'=2}_{\text{radial}}$ (a.u.) [b]
9	−2.954	−2.939	−2.995
10	−2.949	−2.892	−2.980
11	−2.794	−2.871	−2.773
12	−2.599	−2.635	−2.597
13	−2.399	−2.342	−2.403
15.25	−1.985	−2.058	−1.993

[a] Angular parts of $\langle kf|z^2|3p\rangle$ and $L(kf)$ are the same.
[b] Angular part of $\langle kp|z^2|3p\rangle$ equals the sum of the angular parts of $L(kp)^{l'=0}$ and $L(kp)^{l'=2}$.

tions were carried out for linear polarization of the radiation field using Figs. 1(a) and 1(b). For circular polarization the $kf\ ^1D$ and $kp\ ^1D$ results are multiplied by $\frac{3}{2}$ while the $kp\ ^1S$ final state is forbidden by angular momentum selection rules. In order to have the energies for the resonances and thresholds agree as closely with experiment as possible, experimental values from Moore's tables[38] are used for all bound excited-state single-particle energies. The ionization energy of the $3p$ state is 0.579 a.u. (15.755 eV)[38] while the $3s$ removal energy is 1.075 a.u. (29.24 eV).[39] Figures 2–4 cover the energy values from threshold for two-photon ionization, $\omega = |\epsilon_{3p}|/2 = 7.88$ eV, to threshold for single-photon ionization, $\omega = |\epsilon_{3p}| = 15.755$ eV. The denominator associated with the sum over bound states in Eq. (25) will vanish when $\omega = \epsilon_{n'l'} - \epsilon_{3p}$. The resonance peaks of Figs. 2–4 thus extend to infinity since Eq. (25) is evaluated without including shifts and widths (which are flux dependent) in the denominators. The radiation resonance energy corresponds to the energy needed for bound excitation of the atom by a single photon. The resonance peak at $\omega = 11.62$ eV in the partial cross sections for $kp\ ^1D$ and $kp\ ^1S$ in Figs. 2 and 3 results from the excitation of the $3p^5 4s\ ^1P$ state. Intermediate states of Eq. (25) involving s waves are not allowed in lowest order for the $kf\ ^1D$ partial cross section. The $5s\ ^1P$ and $3d\ ^1P$ resonances occur at 14.09 eV and 14.15 eV, respectively. The remaining infinity of bound $ns\ ^1P$ and $nd\ ^1P$ resonances are found between $\omega = 14.15$ eV and the single-photon ionization threshold at 15.755 eV. Calculations were not carried out beyond ω equal to the $3d\ ^1P$ resonance energy. Points were calculated for Figs. 2–4 and 6 at intervals of 0.5 eV starting at $\omega = 8.0$ eV. The diagram component given by Fig. 1(b), for $n = 3p$, $m = 3s$, and $k = kp$ was found to make a relatively small contribution to the $kp\ ^1D$ and $kp\ ^1S$ cross sections when compared to Fig. 1(a).

The matrix element $\langle kl|J|n'l'\rangle$ of Eq. (25) must be known quite accurately in the energy range ω near a $|n'l'\rangle$ state resonance. The radial integration cutoff at $R = 20.365$ is sufficient to accurately evaluate the velocity-matrix elements involving the $4s\ ^1P$, $5s\ ^1P$, and $3d\ ^1P$ states and the length-matrix element for the $4s\ ^1P$ state. For energies ω near the $5s\ ^1P$ and $3d\ ^1P$ resonances, length-matrix elements in Eq. (25) for the $5s\ ^1P$, $6s\ ^1P$, $3d\ ^1P$ and $4d\ ^1P$ states calculated to $R = 20.365$ are replaced by ones calculated to $R = 90.0$. This is an approximate procedure since it disturbs (a 1–30% effect) the balance between the bound and

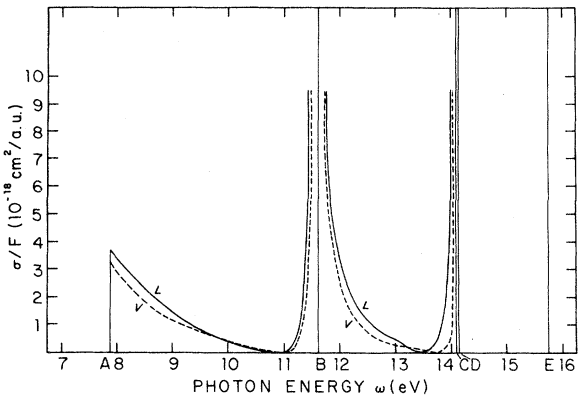

FIG. 2. $kp\ ^1D$ partial cross section (10^{-18} cm^2/a.u. of flux) for the two-photon ionization of the $3p$ shell of argon. The radiation field is linearly polarized. Length (L) and velocity (V) cross sections in second order are shown. The threshold for two-photon ionization is at $\omega = A$; $\omega = B$, C, D are the radiation resonance energies for the $4s\ ^1P$, $5s\ ^1P$, and $3d\ ^1P$ states, respectively; and $\omega = E$ is the single-photon ionization threshold. Calculations were not carried out beyond $\omega = D$.

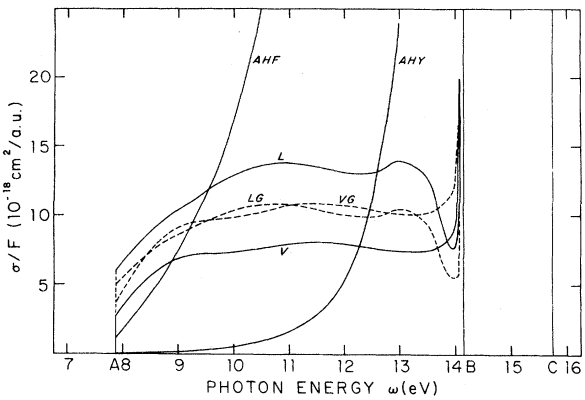

FIG. 4. $kf\ ^1D$ partial cross section (10^{-18} cm^2/a.u. of flux) for the two-photon ionization of the $3p$ shell of argon. The radiation field is linearly polarized. Length (L) and velocity (V) cross sections in second order are shown. Length (LG) and velocity (VG) curves include third-order intrashell ground-state correlations. The AHF and AHY curves are approximate calculations using Eq. (28) with Hartree-Fock and hydrogenic wave functions, respectively. The two-photon threshold is at $\omega = A$, the $3d\ ^1P$ resonance energy at $\omega = B$ and $\omega = C$ is the threshold for single-photon absorption.

continuum contributions needed for the sum rule of Eq. (27). Without this modification, however, the length curve in Figs. 2 and 3 would not show the dip to near zero between the $4s\ ^1P$ and $5s\ ^1P$ resonances. The velocity formulation, on the other hand, should give reliable results near the $5s\ ^1P$ and $3d\ ^1P$ resonances. The radial cutoff at $R = 20.365$ can of course be increased so that more bound matrix elements can be evaluated accurately, but only at the cost of a large increase in the number of mesh points needed for the continuum integral of Eq. (25).

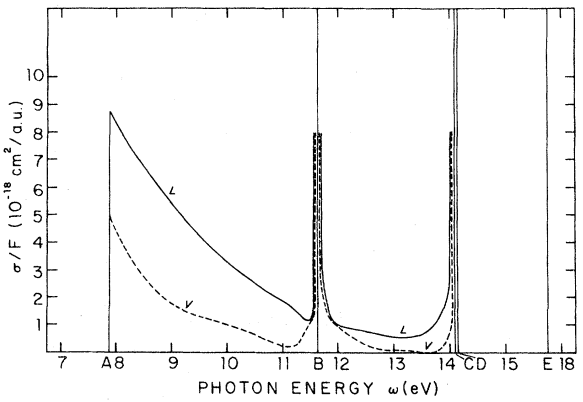

FIG. 3. $kp\ ^1S$ partial cross section (10^{-18} cm^2/a.u. of flux) for the two-photon ionization of the $3p$ shell of argon. The radiation field is linearly polarized. Length (L) and velocity (V) cross sections in second order are shown. The letters A–E have the same meaning as in Fig. 2.

Two approximate results,[8] labeled AHF and AHY, are presented in Fig. 4 for the $kf\ ^1D$ partial cross section. For some set of frequencies $\bar{\omega}(\omega)$ the following equality must hold (in the length form using linear polarization)

$$D(kf) = \frac{\langle kf | z^2 | 3p \rangle}{\bar{\omega}(\omega) + \omega} \quad , \tag{28}$$

where $D(kf)$ is obtained from Eq. (25). $\bar{\omega}(\omega)$ was found to decrease uniformly from $\bar{\omega} = -13.6$ eV at $\omega = 9$ eV to $\bar{\omega} = -21.8$ eV at $\omega = 14$ eV. In the argon results of Bebb and Gold,[8] Eq. (28) was used to solve for $D(kf)$ by choosing $\bar{\omega}(\omega)$ as a constant equal to the first excitation energy of argon. The curves AHF and AHY, calculated by Eq. (28) with $\bar{\omega}(\omega) = \epsilon_{3p} - \epsilon_{3d} = -14.15$ eV, differ only in that AHF uses Hartree-Fock wave functions and AHY uses hydrogenic wave functions. The approximate results are in very poor agreement with the lowest-order $kf\ ^1D$ results obtained using Eq. (25).

The effect of electron correlations on the lowest-order $kf\ ^1D$ partial cross section was investigated. Angular-momentum excitation components of a few of the many third-order diagrams are shown in Fig. 5. The values of l' and l'' are determined from angular selection rules. The intrashell ground-state correlated length and velocity results shown in Fig. 4 (labeled LG and VG) include the $l' = 2$, $l'' = 2$ and $l' = 2$, $l'' = 0$ components of Fig. 5(a)

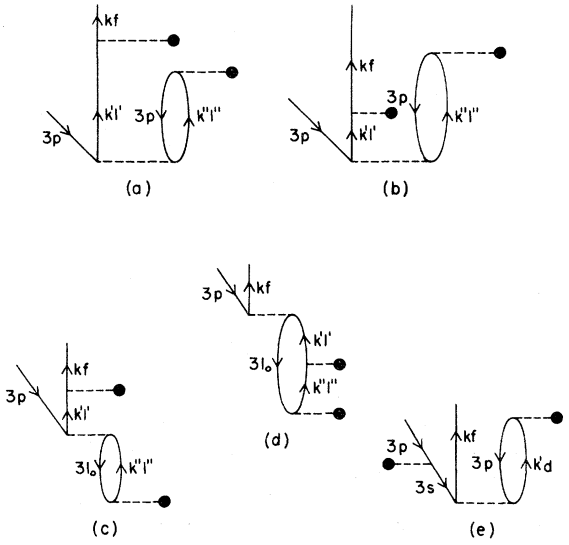

FIG. 5. Excitation components of various third-order diagrams contributing to the $kf\,{}^1D$ partial cross section for the two-photon ionization of argon. Sums over intermediate states labeled by $k'l'$ or $k''l''$ involve bound as well as continuum contributions. Figures (a) and (b) are intrashell components of ground-state correlation diagrams. Figure (c) is an intermediate-state correlation diagram while Fig. (d) is a final-state diagram. Figure (e) involves an interaction on a hole line.

and their exchanges and the $l'=2$, $l''=2$ component of Fig. 5(b) and its exchange. The $l'=2$, $l''=2$ component of Fig. 5(a) and its exchange dominate by an order of magnitude the individual contributions from the other two calculated ground-state components. From previous photoionization calculations of argon[30] we estimate that Figs. 5(a) and (b) are the most important ground-state correlation diagrams.

An intermediate-state correlation diagram is shown in Fig. 5(c). The important intrashell $l_0=1$, $l'=2$, $l''=2$ component of Fig. 5(c) and its associated exchange are cancelled by interactions with the potential and the passive unexcited states as has been previously explained in Sec. II. The intrashell $l_0=1$, $l'=2$, $l''=0$ component of Fig. 5(c), its exchange, and their interactions with the passive unexcited states were calculated and added to the ground-state correlated results. Radiation resonances due to the $n''s\,{}^1P$ states (at $\omega=B$ and D) now enter the $kf\,{}^1D$ partial cross section as shown in Fig. 6 (curves labeled LGI and VGI). Intrashell correlation effects are thus seen to introduce additional resonance structure into the partial cross sections.

The important intrashell $l_0=1$, $l'=3$, $l''=2$ component of the final-state correlation diagram shown in Fig. 5(d) and its exchange are also cancelled by the choice of potential for the radial kf states. The intershell diagram of Fig. 5(e) and its exchange and radial equivalents were calculated and found to be extremely small. There are no radiation resonances due to $3s\,3p^6n''p\,{}^1P$ states since the energy ϵ_{3s} is sufficiently large to prevent the $(\epsilon_{3s}-\epsilon_{n\bar{p}}+\omega)$ part of the denominator of the intershell $l_0=0$, $l'=2$, $l''=1$ component of Fig. 5(c) from vanishing for the energy range of ω considered here.

The intershell $l_0=0$, $l'=2$, $l''=1$ component of the final-state correlation diagram of Fig. 5(d) gives rise to configuration interaction or autoionizing resonances found commonly in photoionization work.[40] The bound $3s\,3p^6nd\,{}^1D$ states for which the $(\epsilon_{3s}-\epsilon_{n'\bar{d}}+2\omega)$ part of the denominator vanishes are degenerate in energy with the continuum $3s^2\,3p^5\,kf\,{}^1D$ states. The approximate location of the $3d\,{}^1D$ autoionizing resonance, shown in Fig. 6 (at $\omega=C$), is obtained semiempirically from Moore's tables.[38] Widths and level shifts for autoionizing resonances in many-body perturbation calculations can be found in the usual way[30,40] by summing certain higher-order terms involving only Coulomb interactions.

The effect of photon radiative corrections on the $kf\,{}^1D$ partial cross section was also investigated. The pure radiative fourth-order diagram of Fig. 1(f) and its three other associated time orderings of the emission interaction may be calculated ap-

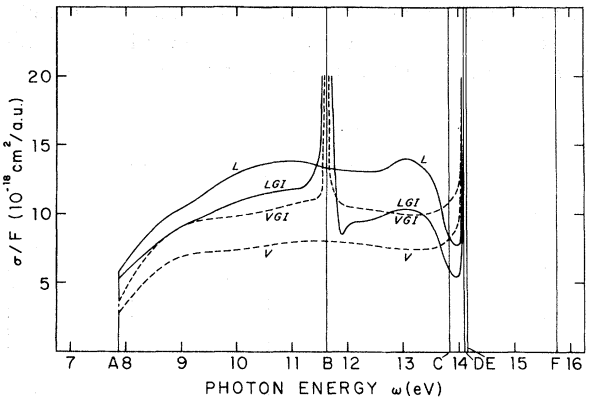

FIG. 6. $kf\,{}^1D$ partial cross section (10^{-18} cm^2/a.u. of flux) for the two-photon ionization of the $3p$ shell of argon. The radiation field is linearly polarized. The length (LGI) and velocity (VGI) curves include contributions from diagrams leading to the $4s\,{}^1P$ and $5s\,{}^1P$ resonances as well as third-order intrashell ground-state correlations. The curves (L) and (V) from Fig. 4 are repeated for comparison. The two-photon threshold is at $\omega=A$, the single-photon threshold at $\omega=F$; $\omega=B$, D, E are the $4s\,{}^1P$, $5s\,{}^1P$, and $3d\,{}^1P$ radiation resonance energies, while $\omega=C$ is the $3d\,{}^1D$ autoionizing resonance energy.

proximately. Figure 1(f) may be given by

$$M_4 = -\frac{2\pi F\omega}{c}\frac{\langle kf|z^4|3p\rangle}{[\bar{\omega}(\omega)+\omega]^2[\bar{\omega}(\omega)+2\omega]}, \qquad (29)$$

which is added to the terms inside the absolute square of a length formulation of Eq. (24). The set of frequencies $\bar{\omega}(\omega)$ are calculated using Eq. (28). Values for $D(kf)$ in Eq. (28) are obtained (at each ω) by summing diagrams from second [Eq. (25)] and third order. It was found that the fourth-order diagram of Fig. 1(f) and its three other time orderings begin to significantly affect the lower-order $kf\,^1D$ cross section results at around a flux F of 10^{32} photons/cm^2 sec (0.07 a.u.).

In the vicinity of a radiation resonance, higher-order photon radiative corrections contribute to the half-width and the level shift in the denominator of the second-order results of Eq. (25).[22,23] At low photon fluxes the widths and shifts are a result of the spontaneous decay of the resonant bound intermediate state. At higher photon fluxes the radiation-field-induced emission and absorption rates yield flux-dependent widths and shifts. The effects of the laser line shape may also become important.[23]

IV. SUMMARY

In calculating the two-photon ionization rate of the argon atom we have sought to examine several effects. An explicit sum over both bound and continuum intermediate states has shown that previous approximate methods can be in serious error when applied to multiphoton processes in atoms other than the alkalis. The inclusion of electron correlations in the two-photon process has introduced the same wealth of phenomena that is found in current photoionization work. Radiation resonances forbidden in the lowest-order partial cross sections have been seen to occur through correlations in higher orders. Autoionizing resonances were found when considering various intershell electron correlation terms. The flux-dependent nature of the two-photon ionization rate was also investigated by approximately calculating certain fourth-order radiation field corrections.

A generalization of the methods used in this paper can be applied to a wide variety of multiphoton processes in both atoms and molecules. The usefulness of adequate approximate methods remains, however, since the number of intermediate states involved in, say, a high n-photon process of an open-shell atom may become prohibitively large. We plan to study other multiphoton processes in future work.

ACKNOWLEDGMENTS

We would like to thank Dr. A. W. Fliflet and Dr. S. L. Carter for helpful discussions.

*Research supported by the National Science Foundation.

[1]M. Goeppert-Mayer, Ann. Phys. (Leipz.) 9, 273 (1931).
[2]G. S. Voronov and N. B. Delone, Zh. Eksp. Teor. Fiz. Pis'ma Red. 1, 42 (1965) [Sov. Phys.—JETP Lett. 1, 66 (1965)].
[3]P. Agostini, G. Barjot, J. F. Bonnal, G. Mainfray, C. Manus, and J. Morellec, IEEE J. Quantum Electron. QE-4, 667 (1968).
[4]R. A. Fox, R. M. Kogan, and E. J. Robinson, Phys. Rev. Lett. 26, 1416 (1971).
[5]G. A. Delone, N. B. Delone, and G. K. Piskova, Zh. Eksp. Teor. Fiz. 62, 1272 (1972) [Sov. Phys.—JETP 35, 672 (1972)].
[6]N. B. Delone, *The Physics of Electronic and Atomic Collisions, Invited Lectures and Progress Report, VIII ICPEAC* (Institute of Physics, Belgrade, 1973), p. 313.
[7]W. Zernik, Phys. Rev. 135, A51 (1964).
[8]H. B. Bebb and A. Gold, Phys. Rev. 143, 1 (1966).
[9]V. M. Morton, Proc. Phys. Soc. Lond. 92, 301 (1967).
[10]Y. Gontier and M. Trahin, Phys. Rev. 172, 83 (1968).
[11]C. S. Chang and P. Stehle, Phys. Rev. A 4, 641 (1971).
[12]F. V. Bunkin and A. M. Prokhorov, Zh. Eksp. Teor. Fiz. 46, 1090 (1964) [Sov. Phys.—JETP 19, 739 (1964)].
[13]H. R. Reiss, Phys. Rev. A 1, 803 (1970).
[14]J. Gersten and M. H. Mittleman, Phys. Rev. A 10, 74 (1974).
[15]C. Schwartz, Ann. Phys. (N.Y.) 6, 156 (1959); C. Schwartz and T. J. Tiemann, Ann. Phys. (N.Y.) 6, 178 (1959).
[16]S. Geltman, Phys. Lett. 4, 168 (1963).
[17]H. B. Bebb, Phys. Rev. 149, 25 (1966); H. B. Bebb, Phys. Rev. 153, 23 (1967).
[18]L. V. Keldysh, Zh. Eksp. Teor. Fiz. 47, 1945 (1964) [Sov. Phys.—JETP 20, 1307 (1965)].
[19]B. A. Zon, N. L. Manakov, and L. P. Rapoport, Zh. Eksp. Teor. Fiz. 61, 968 (1971) [Sov. Phys.—JETP 34, 515 (1972)].
[20]H. R. Reiss, Phys. Rev. Lett. 29, 1129 (1972).
[21]Y. Gontier and M. Trahin, Phys. Rev. A 7, 2069 (1973).
[22]Y. Gontier and M. Trahin, Phys. Rev. A 7, 1899 (1973).
[23]P. Lambropoulos, Phys. Rev. A 9, 1992 (1974).
[24]W. Heitler, *The Quantum Theory of Radiation*, 3rd ed. (Oxford U.P., Oxford, 1954).
[25]S. DeBenedetti, *Nuclear Interactions* (Wiley, New York, 1964).
[26]K. A. Brueckner, Phys. Rev. 97, 1353 (1955); and in *The Many-Body Problem*, edited by C. DeWitt (Wiley, New York, 1959).
[27]J. Goldstone, Proc. R. Soc. A 239, 267 (1957).
[28]M. Gell-Mann and F. Low, Phys. Rev. 84, 350 (1951).
[29]A. Messiah, *Quantum Mechanics* (North-Holland, Amsterdam, 1966), Vol. II.
[30]H. P. Kelly and R. L. Simons, Phys. Rev. Lett. 30,

529 (1973).
[31]G. C. Wick, Phys. Rev. 80, 268 (1950).
[32]G. Baym, *Lectures on Quantum Mechanics* (Benjamin, New York, 1973).
[33]H. P. Kelly, *Advances in Theoretical Physics* (Academic, New York, 1968), Vol. 2.
[34]M. Ya Amus'ya, N. A. Cherepkov, and L. V. Chernysheva, Zh. Eksp. Teor. Fiz. 60, 160 (1971) [Sov. Phys.—JETP 33, 90 (1971)].
[35]T. Ishihara and R. T. Poe, Phys. Rev. A 6, 111 (1972).
[36]H. J. Silverstone and M. L. Yin, J. Chem. Phys. 49, 2026 (1968).
[37]S. Huzinaga and C. Arnau, Phys. Rev. A 1, 1285 (1970).
[38]C. E. Moore, *Atomic Energy Levels*, Nat. Bur. Stds. Circ. No. 467 (U. S. GPO, Washington, D. C., 1949).
[39]K. Siegbahn *et al.*, Nova Acta R. Soc. Sci. Ups. 20, 1 (1967).
[40]A. W. Fliflet and H. P. Kelly, Phys. Rev. A 10, 508 (1974).